

# Hydrothermal base catalysed treatment of Kraft Lignin for the preparation of a sustainable carbon fibre precursor

Malte Otromke<sup>a,b,1</sup>, Peter S. Shuttleworth<sup>c</sup>, Jörg Sauer<sup>a</sup>, Robin J. White<sup>b,\*</sup>

<sup>a</sup> Institute of Catalysis Research and Technology (IKFT), Karlsruhe Institute of Technology (KIT), Eggenstein-Leopoldshafen, Germany

<sup>b</sup> Sustainable Catalytic Materials Group, Division Hydrogen Technologies, Fraunhofer Institute for Solar Energy Systems ISE, Heidenhofstr. 2, 79110 Freiburg, Germany

<sup>c</sup> Instituto de Ciencia y Tecnología de Polímeros (ICTP), Consejo Superior de Investigaciones Científicas (CSIC), Madrid, España

## ABSTRACT

### Keywords:

Lignin  
Kraft Lignin  
Carbon fibres  
Bio-refinery  
Base catalysed depolymerisation

Industrial Kraft Lignin (KL) prepared by LignoBoost® technology was treated via hydrothermal base catalysed depolymerisation (HBCD). KL was dried and divided into methanol soluble and insoluble fractions. The insoluble fraction was treated in 1 M NaOH (aq) at 300 °C. After precipitation with HCl (aq), the solids yield was ca. 60 wt %. These solids demonstrated improved thermal stability and carbon content, increased solubility in MeOH and reduction in polydispersity. With a view to the use of the product in the preparation of carbon-based materials (e.g. carbon fibres (CF)), thermal analysis was undertaken, revealing a lack of a glass transition below the decomposition temperature, excluding melt pinning. However, a high solubility in organic solvents renders the product a suitable candidate for solvent spinning and for the production of renewable low-cost CFs. Additionally, the process generated an oily liquid phase with yields of ca. 10 wt% containing valuable catechol and methylated derivatives.

## 1. Introduction

Lignin represents a significant volume source of renewable aromatic compounds and is one of the main constituents of woody biomass comprising ca. 20–30 wt% of the dry mass (Gargulak et al., 2000). While lignosulfonates are available at ca. 1 Mt/a since the 1970s, there is no market for the majority of the technical lignin, which is Kraft Lignin (KL). This lignin is burnt in pulp mill recovery boilers to cover the energy demand of the mill and recover > 95% of the chemicals used (Ragnar et al., 1999–2014; Tran and Vakkilainen, 2007). There is a potential capacity of bleached and unbleached pulp generated via the Kraft process of ca. 100 Mt. in 2016 (FAO Food and Agriculture Organization of the United Nations, 2015). Taking into account the hard and softwood distribution and assuming that for an undisturbed operation of the recovery boiler a maximum of 75% of the lignin can be withdrawn from the black liquor, this amounts to ca. 30 Mt/a of KL which could act as a chemical feed stock (op. Björk et al., 2015; Gellerstedt et al., 2013). With the appearance of lignin precipitation processes using CO<sub>2</sub> for acidification (e.g. LignoBoost®, LignoForce™, and SLRP®), further market potential and diversification of KL will arise (Kouisni et al., 2012; Lake and Blackburn, 2014; Tomani, 2010). As a consequence of processing, KL is typically a highly condensed

macromolecule, with ca. 80–90% of β-O-4 bonds having been cleaved, accompanied by a three fold increase in phenolic OH group content and C–C bonds (Alekhina et al., 2015a; Alekhina et al., 2015b; Gierer, 1980; Nagy et al., 2010; Rinaldi et al., 2016).

Regarding product development, there is a growing interest in KL as a carbon fibre (CF) precursor. The first patent was filed in 1969 by Nippon Kayaku and the fibre was briefly available as Kayacarbon brand until 1973 (Otani et al., 1969). The relatively low tensile strength of 0.3 to 0.8 GPa could not compete with PAN based fibres and a low oil price prevented lasting success. With a strong market pull for sustainable/renewable materials, the production of CFs from biomass and biomass waste streams is receiving renewed interest (Baker and Rials, 2013); e.g. lignin derived CFs in the automotive industry; non wovens for heat retardants and insulations (Paul et al., 2015). To find large scale adoption, lignin derived CFs must present attractive tensile strength (> 1.72 GPa) and modulus (> 172 GPa) properties with a price between 10 and 15 \$/kg (Baker and Rials, 2013).

Regarding the suitability of KL in CF production, the heteroatom content in the precursor impacts on the carbonisation processes, supposed to result in stabilisation of the fibre and an increased carbon yield (Frank et al., 2014). Nevertheless, many problems occur, including a tendency for lignin to react with itself during (melt) spinning, while

\* Corresponding author.

E-mail address: robin.white@ise.fraunhofer.de (R.J. White).

<sup>1</sup> Present address: Clariant Produkte (Deutschland) GmbH, Group Process Technology, Frankfurt am Main, Germany.

heterogeneity (e.g. in terms of molecular weight profile) can hinder stable spinning of the fibres (Baker and Rials, 2013; Kadla et al., 2002).

During the processing/stabilisation of lignin based fibres, low molecular weight compounds are believed to undergo polymerisation reactions, forming a stable structure for carbonisation (Frank et al., 2014). If the polymerisation reactions do not consume the majority of the low molecular weight compounds during carbonisation, evaporation can also occur, reducing yield and resulting in hole formation in the fibre matrix (i.e. reducing tensile strength) (Mainka et al., 2015a). While the aforementioned Kayacarbon CFs were dry spun with poly(vinyl alcohol) as copolymer, current research indicates interest in the use of melt spinning (Baker et al., 2012; Kadla et al., 2002; Sudo and Shimizu, 1992). Therefore, any lignin used must have a glass transition temperature well below its decomposition temperature and not change its physical properties while being held in the glassy state. The high phenolic OH group content of KL makes this a problematic task. With regard to reducing heterogeneity and establishing a usable glass transition temperature, Baker et al. have performed extractions and developed a proprietary process using organic solvents in order to purify a hardwood KL and increase its melt spinnability (Baker et al., 2012). This decreased the glass transition temperature from 202 to 128 °C facilitating melt spinning, although a complete stabilisation of the fibre was not possible and fibre fusing as well as evaporation during carbonisation was observed (Baker et al., 2012).

Processing of lignin leading to an increase in thermal stability and “degree” of molecular/structural condensation, while at the same time yielding a more homogeneous molecular weight distribution, would be of significant interest. Hydrothermal base catalysed processes (HBCD) that use 1 M NaOH (aq) as solvent at temperatures of ca. 300 °C and retention times of ca. 15 min are promising for altering technical lignin in the desired way (Beauchet et al., 2012; Erdocia et al., 2014; Katahira et al., 2016; Mahmood et al., 2013; Miller et al., 2002; Roberts et al., 2011; Schmiedl et al., 2012; Toledano et al., 2014). HBCD could be integrated into existing Kraft mills, since it employs existing technology and the chemicals required can be recovered in the mill's own recovery cycle. In this paper, an HBCD process is investigated with the aim to optimise KL conversion for CF production. This is based on softwood KL originating from the Domtar, Plymouth, NC, USA pulp mill. This softwood KL is initially treated in a polar, organic solvent, namely methanol (MeOH), to extract the volatile low molecular weight fraction. The insoluble fraction from this extraction is treated under HBCD conditions to increase the degree of molecular/structural chemical condensation and homogeneity.

## 2. Material and methods

### 2.1. Chemicals

Lignin was supplied via UPM Biofore ([www.upmbiofore.com](http://www.upmbiofore.com)), Finland, originating from the Domtar pulp mill in Plymouth, NC, USA, as precipitated via the LignoBoost® technology (ca. 30 wt% H<sub>2</sub>O content). Before use, it was dried at 80 °C under vacuum for 24 h. The trees used for production at the pulp mill are northern pine, i.e. softwood. MeOH (Emsure, +99.9%), acetone (Technic France, 99%), ethyl acetate (Carl Roth, 99.9%), guaiacol (Acros, +99%), catechol (Alfa Aesar, 99%), phenol (Alfa Aesar, 99%), syringol (Sigma Aldrich, 99%), 3 methoxycatechol (Sigma Aldrich, 99%), 4 methylcatechol (Alfa Aesar, 96%), 3 methylcatechol (Sigma Aldrich, 99%), 4 ethylcatechol (Sigma Aldrich, 99%), 4 ethylguaiacol (Sigma Aldrich, 99%), vanillin (Sigma Aldrich, 99%), acetovanillone (Sigma Aldrich, 98%), homo vanillic acid (Sigma Aldrich, 99%), NaOH (Carl Roth, 99%), Na<sub>2</sub>SO<sub>4</sub> (Carl Roth, 99%), HCl (Carl Roth, 32%), and DMSO *d*<sub>6</sub> (Carl Roth, 99.8 atom%D) were used as procured.

### 2.2. Methanol extraction from lignin

The extraction procedure was performed in a 45 mL centrifuge vial at room temperature and ambient pressure under vigorous shaking. After shaking, the mixture was left to mature for a further 2 h. This was followed by centrifugation at 9000 rpm (RCF = 7510) for 5 min and subsequent decantation. The procedure was performed once. Extractions were conducted at different lignin concentrations (10 wt%, 20 wt%, 30 wt%) to see if concentration increases linearly. Additionally, a sequential dissolution of KL in MeOH was conducted to estimate the maximum number of aromatic compounds dissolvable in MeOH. The feed solution for the HBCD step was prepared at a concentration of 250 mg mL<sup>-1</sup>. The two fractions obtained from each separation step were dried under vacuum at 60 °C for 24 h and analysed via GPC, EA, TGA, GC MS FID, 2D HSQC NMR, <sup>13</sup>C CP MAS NMR, and ATR FT IR.

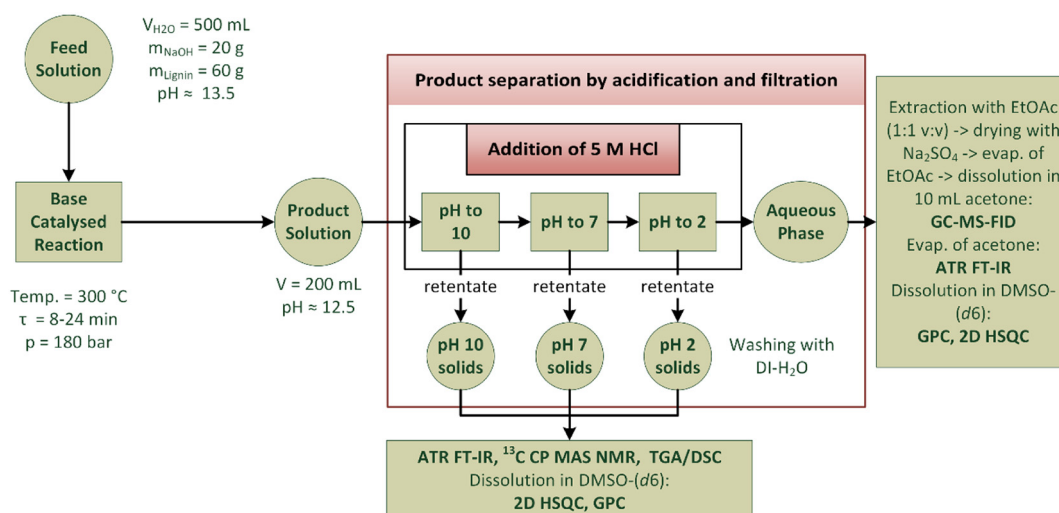
### 2.3. Continuous hydrothermal reactions

The continuous reaction rig is shown in Fig. S1. As feed containers, 1 L HPLC bottles were used. These were pressurised with N<sub>2</sub> to 0.1 bar to prevent the pump from running on gas and a 10 µm stainless steel filter prevents particles from clogging the pump. A Knauer Smartline 1000 HPLC pump with piston heads for a max flow rate of 10 mL/min was used. A tube in tube heat exchanger was installed before the feed enters the reactor. To improve heating rate, the final 25 cm of the heat exchanger was heated via an electrical heating chord set at 50 K below the desired reaction temperature. The reactor was U shaped in geometry to maximise reaction volume in the limited space of the oven. Fig. S2(a) shows an exemplary temperature profile as a function of volume. The first and the last point of measurement are outside the reactor giving the temperatures at the end of the pre heating track and the entrance of the cooling track, respectively. Oven temperature was adjusted, so that thermocouple No. 4 (at ca. 40 mL) was set at 300 °C. With increasing flow rates, this led to a flattened curve profile. This is explained by the laminar flow inside the tubes and the resulting non optimal heat transfer. The total reactor volume is 50 mL and retention times for the kinetic runs were calculated based on this volume. Reactor pressure was controlled via an overflow valve (OFV 1) set at 180 bar. Gas and liquid phases were separated on the low pressure side (1.2 bar) and both phases were sampled for analysis. An optical sensor (LIC 1) was used to control the liquid level in the phase separator and enable liquid sample withdrawal via the magnetic valves (MV 1.3). Over pressure at the low pressure side was controlled with a pressure regulation valve (PRV) and loss of pressure was compensated via a differential pressure valve (OFV 2) adding N<sub>2</sub> if needed. Reactor and periphery were made of X6CrNiMoTi17.12.2 steel (AISI 316Ti or DIN 1.4571).

The test rig was filled with 1 M NaOH (aq) prior to each reaction run which is displaced by the feed solution. Retention time characterisation was performed to determine the time after which the first sample could be taken. Therefore a 1 wt% guaiacol solution in H<sub>2</sub>O was used to generate a Heaviside step response. The concentration at the outlet was measured via GC FID as a function of retention time and compared to the signal of the feed solution. Fig. S2(b) shows the value of  $c(t)/c_0$  versus  $\Theta$ , where  $c(t)$  is the concentration of guaiacol at the outlet at time  $t$  and  $c_0$  is the concentration of the feed solution.  $\Theta$  is the dimensionless retention time and given by  $\Theta = \dot{V} \Delta t V^{-1}$ .  $V$  is the volume of the total test rig including reactor and periphery and was measured to be 190 mL. For the reaction runs, the value for  $\Theta$  was set to 1.50, i.e. sampling for runs with  $\dot{V} = 3.125$  mL/min started after 91.2 min. All reactions were performed at 300 °C and 180 bar.

### 2.4. Feed preparation and product treatment

An overview of the process and associated analytics is provided in



**Scheme 1.** Product work-up procedure for the reactions under basic hydrothermal conditions.

Scheme 1. The feed solution was prepared using 1 M NaOH (aq) and dissolution of the solid lignin derived compounds at a ratio of  $m_{\text{lignin}}:m_{\text{NaOH}} = 3:1$ . Density and pH of the feed were recorded. For product analysis 200 mL was taken from each run and the density and pH measured. The pH was lowered to 10 by adding 5 M HCl (aq) in portions of 0.5 to 1.0 mL under measurement with a pH probe. The sample was stirred during the procedure and, after reaching the desired pH, filtered by vacuum filtration through a Büchner funnel. The solid residue was thoroughly washed with deionised (DI) H<sub>2</sub>O and dried. The pH of the filtrate was then further lowered to pH 7 and pH 2, respectively. The filterability of the pH 10 dispersion was poor, resulting in the need to centrifuge the sample. The solid remains were then re-dispersed in DI H<sub>2</sub>O and the pH lowered to 2 with 5 M HCl (aq). Solid samples were dried after washing under reduced pressure at 80 °C for 24 h. Their masses were recorded and analysed via GPC, EA, TGA, <sup>13</sup>C NMR, and ATR FT IR. The pH 2 aqueous phase was extracted with ethyl acetate (EtOAc, 1:1, v:v) and the EtOAc phase dried with Na<sub>2</sub>SO<sub>4</sub>. EtOAc was then evaporated under reduced pressure at 40 °C and the mass of the resulting oil recorded. This oil was dissolved in 10 mL acetone and an aliquot of 1.5 mL analysed via GC MS FID. From the remaining solution, acetone was again evaporated and the resulting oil further analysed by GPC, NMR, and ATR FT IR. The aqueous phase after extraction was dried under ambient conditions and acetone used to extract remaining organic compounds in the NaCl. Acetone was used as NaCl has a very low solubility.

## 2.5. Analytics

All data files were typically exported as .ascii or .txt files to allow processing and preparation of image files with OriginPro® v9 software.

### 2.5.1. Gel permeation chromatography (GPC)

The pump (515), auto sampler (717 plus), column oven, refractive index (RI) detector (2414), and dual  $\lambda$  absorbance detector (2487) were all manufactured by Waters, Milford, MA, USA. The GPC columns were of a poly hydroxy methacrylate copolymer (Polymer Standards Services GmbH, Mainz, Germany). Columns used were Suprema 20  $\mu\text{m}$  pre column; Suprema 1000 20  $\mu\text{m}$ , 8 mm I.D.  $\times$  300 mm, 100 1,000,000; Suprema 100 20  $\mu\text{m}$ , 8 mm I.D.  $\times$  300 mm, 100 100,000. Prior to analysis, samples were dissolved at a concentration of 2 mg mL<sup>-1</sup> in DMSO with 0.1 M LiBr. Solutions were held at 80 °C for 60 min and matured for 24 h under continuous shaking at room temperature. GPC Detection was performed using a UV detector at  $\lambda = 280$  nm and an RI detector. The GPC was calibrated based on pullulan standards over the

range of 180 1,540,000 g/mol.

### 2.5.2. Elemental analysis (EA)

EA was performed at the chemical laboratory of the University of Freiburg, Germany using a Vario EL Element Analyser. 1.5 mg of sample was analysed in CHNS mode.

### 2.5.3. Thermogravimetric analysis (TGA/DTG)

TGA was performed using a Pyris 1 TGA (Perkin Elmer) equipped with a standard furnace under a N<sub>2</sub> flow rate of 20 mL/min. TGA was also performed using a TA Instruments Q50, under a flow rate of 60 mL/min N<sub>2</sub>. In both cases samples were equilibrated at 50 °C and ramped to 800 °C at 10 K min<sup>-1</sup>.

### 2.5.4. Differential scanning calorimetry (DSC)

DSC was performed using a Perkin Elmer DSC 7 device. Samples were heated to 100 °C and then heated to the specified temperature, cooled to 100 °C to minimize moisture absorption, and the second heating was recorded. A temperature ramp of 5 °C min<sup>-1</sup> was used. Samples were analysed in sealed aluminium analysis pans, with a pin hole made in the top of the pan. Pans were re weighed after analysis and mass values modified accordingly. To determine the glass transition temperature, the TA Universal Analysis software was used.

### 2.5.5. Gas chromatography (GC)

GC was qualitatively performed on a GC MS (Agilent Technologies 5975C, one column: HP 5 ms: 30 m  $\times$  250  $\mu\text{m}$   $\times$  0.25  $\mu\text{m}$ ) and quantitatively via a GC FID (Agilent Technologies 7890A, one column: DB 5 ms: 30 m  $\times$  250  $\mu\text{m}$   $\times$  0.5  $\mu\text{m}$ ). The carrier gas used in both devices was helium, with a total flow rate of 27.6 mL/min. The temperature ramping program of the GCs started with an isothermal time of 6 min at 35 °C followed by a temperature increase to 270 °C at 5 °C min<sup>-1</sup> and a final isothermal time of 5 min. For a first qualification, the NIST data base was used; the results were then verified based on known standards. Quantification was performed with 1 mg mL<sup>-1</sup> syringol in acetone in sandwich injection mode. Front inlet temperature was set at 280 °C with an applied splitting ratio of 5:1. The injection volume was 1  $\mu\text{L}$  for both samples and standards.

### 2.5.6. Fourier transform infrared spectroscopy (FT IR)

Spectra were acquired using on a Bruker Vertex70 equipped with an attenuated total reflectance (ATR) cell fitted with a germanium crystal. Spectra were acquired using 128 scans over the wavenumber range of 4000 to 650 cm<sup>-1</sup>, at a resolution of 4 cm<sup>-1</sup>.

### 2.5.7. $^{13}\text{C}$ cross polarisation magic angle spinning (CP MAS) NMR

Solid state  $^{13}\text{C}$  CP MAS NMR spectra were obtained using a Bruker AV 400 WB device. Prior to analysis, samples were freeze dried. 120 mg of sample were weighed and 12 mg of sodium trimethylsilyl propionate (TMS<sup>+</sup>P) was added as an internal standard. The spectra were recorded at 100.56 MHz with an acquisition time of 40.6 ms and 3600 scans were recorded.

### 2.5.8. 2D heteronuclear single quantum correlation (HSQC) NMR in DMSO $d_6$

2D HSQC NMR spectra were acquired using a Bruker Avance III 400. Samples ( $150\text{ mg mL}^{-1}$ ) were prepared for analysis by dissolution in DMSO  $d_6$ . The spectra were recorded at 400 MHz with an acquisition time of 183.0 ms and 100 MHz and 15.9 ms for  $^1\text{H}$  and  $^{13}\text{C}$  respectively. Total number of scans was 32. The samples were dissolved over 24 h at a concentration of  $150\text{ mg mL}^{-1}$ . No visible solid residue could be detected. The collected data was Fourier transformed with the software ACD/NMR and the resulting matrix exported to an ASCII file. Using MatLab<sup>®</sup>, normalisation and integrations were performed. The size of the matrix (defined by the resolution of the 2D NMR) was set at  $1024 \times 1024$  and the scanned area ranged from  $\delta_{13\text{C}} = 0.2$  to  $159.81$  ppm and is for most  $\delta_{1\text{H}}$  from  $-2$  to  $10$  ppm. This results in a resolution of  $\Delta\delta_{13\text{C}} = 0.156$  ppm and  $\Delta\delta_{1\text{H}} = 0.012$  ppm. Normalisation is performed by searching the defined DMSO area for its highest value and then dividing the whole matrix by this number. For integration, the noise of the results' matrices is removed by setting all values below the defined noise level to 0, i.e. only values above a certain value are considered for integration.

### 2.5.9. $^1\text{H}$ NMR in DMSO $d_6$

The NMR measurements were performed on the same machine as the 2D HSQC.  $^1\text{H}$  NMR spectra were acquired at 400 MHz, 32 transients, and an acquisition time of 4.09 s.

## 3. Results & discussion

### 3.1. Methanol extraction

The extraction lead to a MeOH soluble low molecular weight fraction (denoted as LMW) and an insoluble high molecular weight fraction (denoted as HMW). Dissolution of 10, 20, and 30 wt% lignin in MeOH lead to percentages of LMW of 40, 23, and 34, respectively. This indicates that the amount of lignin dissolved reduces with increasing concentration and increases again with a change in nature of the solvent, i.e. at higher lignin concentrations. The aim of the extraction process was to remove volatile compounds from the lignin in order to reduce damage to the matrix during stabilisation/carbonisation (Mainka et al., 2015a). For the preparation of HBCD feed,  $250\text{ mg mL}^{-1}$  (KL in MeOH) was chosen, since the amount of LMW reached a minimum of ca. 20 wt%.

#### 3.1.1. GPC, EA, and TGA/DSC

The observed changes in molecular weight distributions as

**Table 1**

Gel permeation chromatography, elemental analysis and thermogravimetric data of the KL and high (HMW) and low (LMW) molecular weight extracts.

Sample/fraction	Gel permeation chromatography data			Elemental analysis data					Thermogravimetric analysis data		
	$M_w$ [g/mol]	$M_n$ [g/mol]	PDI [ ]	C [%]	H [%]	$\text{O}^a$ [%]	N [%]	S [%]	$T_d^c$ [°C]	Maximum in DTG [°C]	Residual mass at 600 °C [%]
KL	5330	940	5.7	62.13	5.74	30.39	n.d. <sup>b</sup>	1.74	299.7	359.7	50.1
HMW	7460	1170	6.4	64.55	5.79	28.22	n.d.	1.44	297.3	363.0	52.3
LMW	2320	700	3.3	61.59	5.67	30.88	n.d.	1.86	272.7	352.7	45.4

<sup>a</sup> Calculated by difference.

<sup>b</sup> Not detected.

<sup>c</sup> Temperature at 10% weight loss.

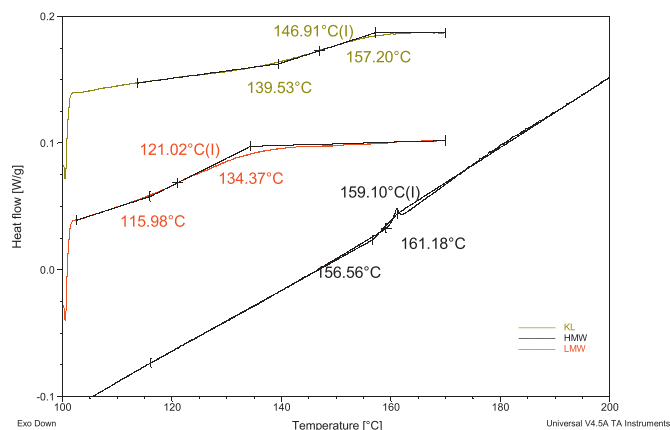


**Fig. 1.** DSC traces of the fractions KL, HMW, LMW. Glass transition temperatures were determined using TA Instruments Universal software within the indicated limits.

determined via GPC (Table 1) indicate an increase in  $M_w$  by 40% for the HMW fraction while the LMW fraction exhibits a decrease by 56%.

Elemental analysis indicates an increase of carbon and decrease in sulphur content in the MeOH soluble fraction (Table 1). It seems that more of the sulphur is bound in larger aromatic structures not being dissolvable in MeOH at the given concentration. Jiang et al., 2017 and Mörck et al., 1986 experienced the same increase in carbon content in the lower molecular weight fractions, while no differences in sulphur content between the fractions could be seen in the work of Jiang et al., where Mörck et al. saw an increase in the lower molecular weight fractions.

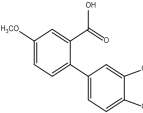
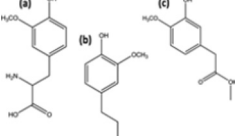
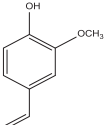
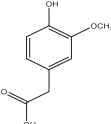
Results of the thermal analysis (TGA) of the three fractions (KL, HMW, LMW; Table 1 and Fig. S3) show that after heating to  $600\text{ °C}$  the LMW has a residue of 45.4 wt%, while HMW and Lignin have 52.3 and 50.1 wt%, respectively. The numbers indicate a higher thermal stability of the HMW fraction, while the LMW fraction exhibits a larger loss in mass. The DSC of the three fractions provides information on the glass transition temperatures ( $T_g$ ) of the samples (Fig. 1). While KL and LMW exhibit a clear glass transition at 147 and  $121\text{ °C}$ , respectively, the HMW fraction only shows a small endothermic event at  $159\text{ °C}$ . Baker et al. used an organic solvent in a proprietary process for purifying a hardwood lignin, thereby decreasing the  $T_g$  from  $130$  to  $88\text{ °C}$  (Baker et al., 2012), i.e. they also experienced a decrease in  $T_g$  for the organics soluble fraction.

#### 3.1.2. GC MS/GC FID

GC only gives information on monomers and some dimers dissolved in MeOH. Since the HMW fraction is not dissolvable in MeOH by definition, compounds detectable via GC are below 1 wt%. GC detectable compounds for KL and LMW are 10 and 25 wt%, respectively. Table 2 shows the main compounds in KL and LMW detectable by GC, indicating an accumulation within the LMW.

**Table 2**

Main compounds in KL and LMW detected via GC-MS-FID.

Compound	Structural formula	Amount [wt%]	
		KL	LMW
E.g. 4-Methoxy-4',5'-methylenemethoxybiphenyl-2-carboxylic acid		3.3 <sup>a</sup>	7.8
E.g. (a) 3-Hydroxy- <i>o</i> -methyltyrosine (b) 4-Propylguaiacol (c) Methyl 4-hydroxy-3-methoxyphenylacetate		1.5 <sup>a</sup>	3.8
Vinyl guaiacol		0.6	0.7
Homovanillic acid		0.3	0.4

<sup>a</sup> Proposed molecular structures as derived from GC-MS analysis and based on probabilities issued from the associated NIST compound database.

### 3.1.3. ATR FT IR

ATR FT IR was used to further analyse the products (Table S1), with band assignments based on previously reported work (e.g. Faix, 1992; Lupoi et al., 2015). The most pronounced bands shown in Fig. S4(A) are 6, 7, 10, 11, 12, and 14, associated with ring modes of guaiacyl units (G units). Bands 3, 4, and 5 belong to C=O stretches and -COOH groups. Band 8 is a combination of the CH deformation in -OCH<sub>3</sub> groups and -CH in plane modes of aromatics. Band 9 represents aliphatic C-H stretches in -CH<sub>3</sub> (excluding -OCH<sub>3</sub>) additional to phenolic OH stretches. 13 is assigned to secondary alcohols and esters in aliphatics. Band 15 is the out of plane deformation of ethylene like groups and 16 is a general aromatic -CH out of plane mode. Bands 17 and 18 are CH out of plane modes special for G units at C<sub>2</sub>, C<sub>5</sub>, and C<sub>6</sub>. In the HMW fraction bands 3 and 4, corresponding to the C=O stretch, are less defined. Here, the KL has three defined FTIR spectral bands, reflecting the larger area of the <sup>13</sup>C CP MAS at  $\delta_{13C} > 190$  ppm. Band 12 is less pronounced in the LMW fraction, which leads to a clearer appearance of a band at 1123 cm<sup>-1</sup>, which can be seen as a small shoulder in the KL and HMW spectra. Band 12 corresponds to the C-H stretch in guaiacyl rings but cannot be taken as a sole indicator for a lesser number of G units. The band at 1123 cm<sup>-1</sup> is also an aromatic ring absorbance. Bands at 5, 6, 7, 10, 11, 12, 14, 17, and 18 are all directly related to G units. Band 8 is also less pronounced in the LMW fraction which corresponds to -OCH<sub>3</sub> groups in aromatics.

### 3.1.4. <sup>13</sup>C cross polarisation magic angle spinning (CP MAS) NMR

<sup>13</sup>C CP MAS NMR analyses of the KL, LMW, and HMW are presented with resonance/chemical shift assignment provided (Fig. S4(B) and Table 3).

The lignin contains significant amounts of carboxylic acids and aldehydes, which could already be assumed from the GC analysis. The <sup>13</sup>C NMR shows that these end groups not only appear in the mono and dimeric fraction, since there is no difference between the LMW and HMW fraction. The use of the derivatisation agent (TMSP; 9 wt%) increases the complexity of the spectrum (i.e. additional -Si(CH<sub>3</sub>)<sub>3</sub>), with associated resonances found in the aliphatic side chains region (-CH<sub>2</sub>- at 30 ppm) and one in the carboxylic acid region (-COO Na<sup>+</sup> at ca. 170 ppm). The region of  $\delta_{13C} > 160$  ppm of the original KL is

**Table 3**Chemical shift assignments for the <sup>13</sup>C NMR analysis of lignin.

Chemical shift [ppm]	Assignment (with the data from Kringstad and Mörck, 1983) (Kringstad and Mörck, 1983)
190 +	G CHO, G CH=CH CHO
175-185	COOH
148.4	C <sub>3</sub> in guaiacyl
131.1	C <sub>1</sub> in guaiacyl
124.6	C <sub>5</sub> in guaiacyl, substituted (C <sub>5'</sub> p, o'-stilbenes)
116.5	C <sub>5</sub> G CH=CH, G CH, G CH <sub>2</sub>
84.2	C <sub>β</sub> in β-aryl ethers
72.8-75.7	C <sub>2-4</sub> xylan
56.1	OCH <sub>3</sub>
35.8	Mainly -CH <sub>2</sub> - in guaiacyl side chains
12.7	CH <sub>3</sub>
0	TMSP

integrated ca. four times larger compared to LMW or HMW for reasons unknown to the author. The remaining spectrograms are comparable in shape and size, while it has to be hinted at some differences. The resonance at  $\delta_{13C} = 131.1$  ppm representing the C<sub>1</sub> in guaiacyl is less pronounced in KL while at 84.2 ppm a resonance with increased intensity is clearly visible in that fraction, which corresponds to the C<sub>β</sub> in β aryl ethers. In the range of  $\delta_{13C} = 72.8-75.7$  ppm lie the C<sub>2-4</sub> carbon atoms of xylan, meaning that some hemicellulosic sugars are still present. The  $\delta_{13C} = 56.1$  ppm resonance represents the guaiacylic methoxy groups (syringylic units are not present) and the aliphatic side chains can be found on lower chemical shifts. The resonance at ca.  $\delta_{13C} = 35$  ppm is corresponding to the two -CH<sub>2</sub>- groups of the TMSP.

12 mg of TMSP were added to 120 mg of lignin. M<sub>TMSP</sub> is 127.3 mg mmol<sup>-1</sup> and the resonance at  $\delta_{13C} = 0$  ppm is corresponding to the -Si-(CH<sub>3</sub>)<sub>3</sub> groups. I.e., the signal corresponds to 0.282 mmol of carbon atoms. Resonances at  $\delta_{13C} = 148.4$  and 56.1 ppm represent the carbon atoms in the guaiacyl ring where the methoxy group is bound to and the carbon atom of the methoxy group, respectively. Taking these values as a measure for the total number of guaiacyl subunits, it gives ca. 0.64 mmol in 120 mg of sample. With a molar mass of 124.1 mg mmol<sup>-1</sup> this represents 77 mg or ca. 65 wt% of the KL. This

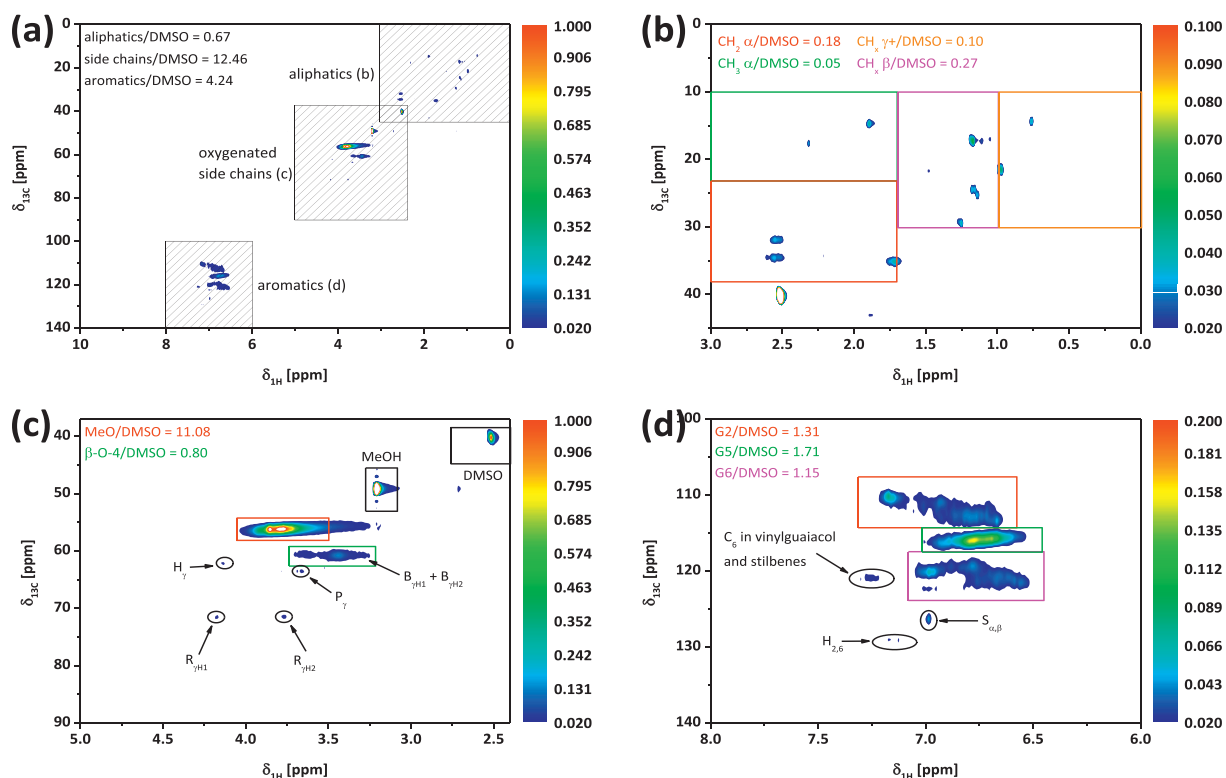


Fig. 2. 2D HSQC NMR spectra of KL. (a) Overview with the three distinct areas and their respective integrated values in relation to the DMSO value, (b) aliphatics region, (c) oxygenated side chains, and (d) aromatics.

value is comparable in all three fractions, but the resolution of resonances in the  $^{13}C$  CP MAS spectra does not allow further differentiation in more detail. When 65% is the mass of guaiacyl units in KL, the remaining 35% make up for the remainder, i.e. mostly side chains. With a mass of 124 g/mol per guaiacol this leads to an average mass of 190 g/mol of one guaiacylic ring with attached side chains.

### 3.1.5. 2D heteronuclear single quantum correlation (HSQC) NMR in DMSO $d_6$

Assignment for the 2D HSQC signals was done with data from various sources (Table S2 and Fig. S5 associated structures) (Constant et al., 2016; Feng et al., 2016; Fernandez Costas et al., 2014; Mainka et al., 2015b; Mattsson et al., 2016; Rencoret et al., 2009; Samuel et al., 2011). From these data, values for the integration of specific areas have been derived (Table S3). Figs. 2, 3, and 4 provide an overview of the 2D HSQC spectra of the KL, HMW, and LMW, respectively. Specific areas have been integrated and set into relation with the DMSO  $d_6$  resonance. In general, the resonances are more distinct and the areas larger in the order LMW > KL > HMW. This can be attributed to more C–H correlations per mass being present in the smaller molecules. The larger molecules are more condensed, thus containing more fused rings and C–C bonds.

$^1H$  NMR analysis supports these findings further, although the differences are less pronounced. The usage of the DMSO  $d_6$  as an internal standard is only semi quantitative, since the amount of deuteration is given as > 99.8%. GC FID analysis of the oil fraction after reaction demonstrated the predominance of vanillin and acetovanillone. The concentration of both compounds was determined with usage of an internal standard. With this information and the analyses of the oil fraction by 2D HSQC a deuteration of 99.93% was calculated. Assuming a concentration of C–H correlations of  $9.9 \mu\text{mol mL}^{-1}$  in the DMSO  $d_6$  (density  $1.19 \text{ mg mL}^{-1}$ ,  $M = 84.17 \text{ g/mol}$ ) and that all correlations in the measured spectra have comparable absorption, quantification can be performed. It has to be kept in mind, that the size of error is

probably > 10%.

The HSQC in Figs. 2(d), 3(d), and 4(d) shows distinct areas for  $G_2$ ,  $G_5$ , and  $G_6$  and that the three areas are overlapping for the  $^1H$  shift. Quantification via HSQC is difficult and requires high signal to noise ratios and the correct settings for the NMR (Constant et al., 2016), but with the aforementioned method, an estimation can be done. The  $G_5$  position has the largest area followed by  $G_2$  and  $G_6$ . This is also true for the HMW and LMW fractions, meaning that condensation and/or attachment of side chains as e.g.  $-CH_3$  and  $-CH_2-CH_3$  mainly occurs at the 2 and 6 positions during pulping. Figs. 2(c), 3(c), and 4(c) show the methoxy groups (MeO) of the guaiacyl units and other oxygenated side chains. The amount of MeO is again higher in the LMW fraction, suggesting that the larger molecules contain less MeO groups. With the information from the EA and the HSQC a  $C_9$  formula, MeO and  $\beta$  O 4 content can be determined (Table S4). Using a  $C_9$  formula is common for lignin and performed in various sources for different kinds of lignin (Alekhina et al., 2015a; Hu et al., 2016). While it is useful for native lignin comprising of phenyl propanoid units, the condensed structure of technical lignin may lead to a repetitive unit with less carbon atoms. The value between two and four for  $\beta$  O 4 linkages lies within the range for KLs in the literature, while the amount of methoxy groups is ca. half the value reported (Gellerstedt, 2015; Hu et al., 2016).

Figs. 2(b), 3(b), and 4(b) give information on non oxygenated side chains. The majority of signals appear in a region where  $CH_x$  in the  $\beta$  position of the ring can be found, thus indicating alkylation with at least two carbon atoms. This is underlined by the majority of alkyl chains in  $\alpha$  position being  $CH_2$  groups.

### 3.2. Hydrothermal base catalysed treatment

Five runs were performed with their conditions given in Table 4. The first three runs #B1–3 were done under the same conditions in order to estimate an error of the complete procedure. These runs used the HMW fraction as feed, while run #B4 used LMW as feed and #B5

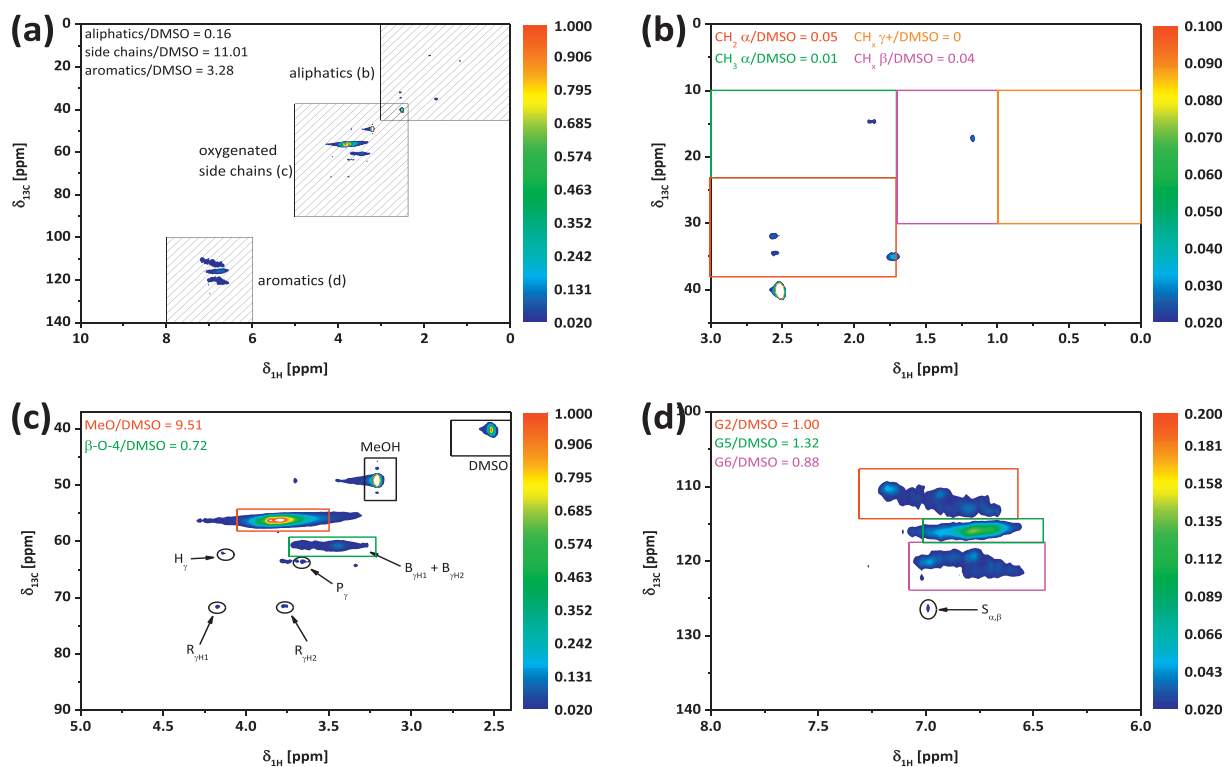


Fig. 3. 2D HSQC NMR spectra of HMW. (a) Overview with the three distinct areas and their respective integrated values in relation to the DMSO value, (b) aliphatics region, (c) oxygenated side chains, and (d) aromatics.

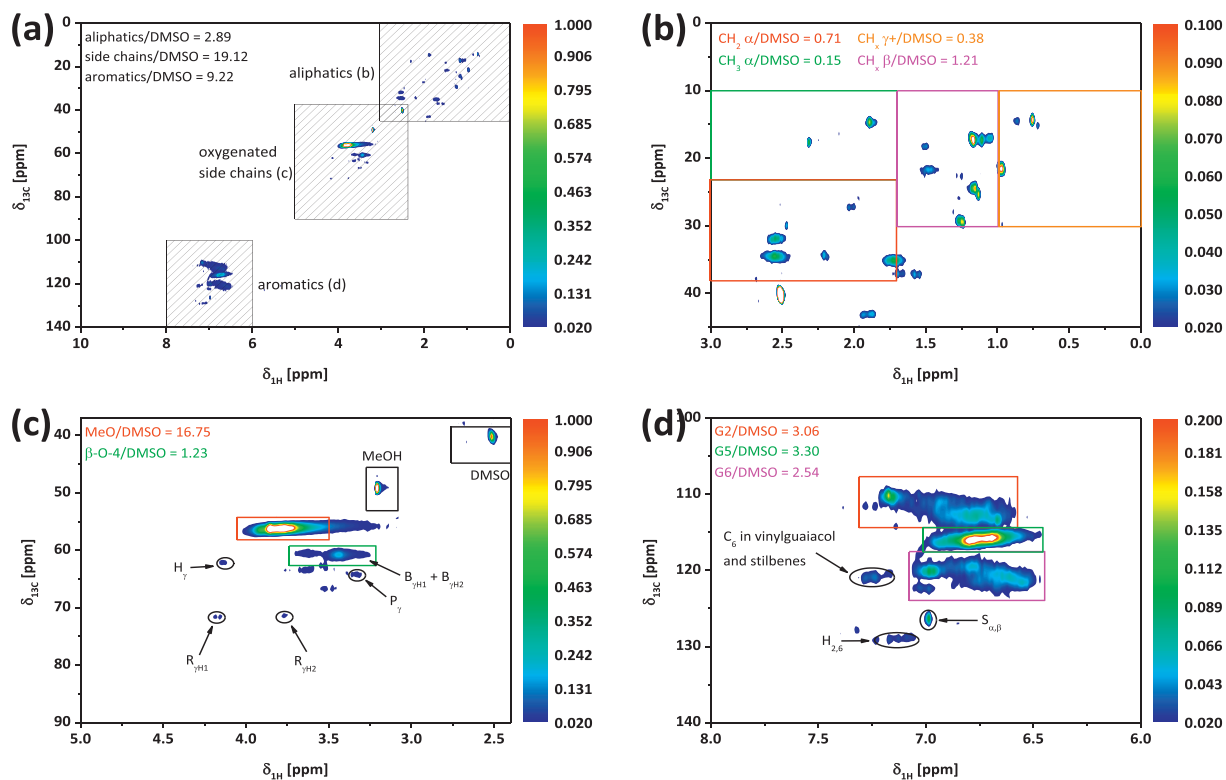


Fig. 4. 2D HSQC NMR spectra of LMW. (a) Overview with the three distinct areas and their respective integrated values in relation to the DMSO value, (b) aliphatics region, (c) oxygenated side chains, and (d) aromatics.

**Table 4**

pH, density, and yields of the different fractions of the runs #B1–5.

Run	Feed	Flow rate [mL/min]	$t_{\text{retention}}$ [min]	pH		$\rho$ [g/mL]		Mass fraction [%]				
				Before	After	Before	After	pH 10	pH 7	pH 2	Oil	Total
#B1	HMW	3.125	16	13.57	12.34	1.047	1.045	58.70	2.94	18.87	10.51	91.02
#B2	HMW	3.125	16	13.43	12.89	1.054	1.056	63.47	3.52	17.32	9.29	93.60
#B3	HMW	3.125	16	13.68	12.58	1.049	1.049	62.66	2.48	13.79	8.54	87.47
#B4	LMW	3.125	16	13.99	13.68	1.049	1.048	61.69	2.48	13.52	12.80	90.49
#B5	KL	3.125	16	14.09	14.02	1.046	1.046	68.45	1.28	7.45	9.97	87.16

KL. Table 4 gives pH and density before and after reactions, as well as the yields of the different fractions. The majority with ca. 60 wt% are solids precipitated at pH 10. Solids precipitated between pH 10 and 7 are only 2–3 wt% and have been excluded from further analyses. The second largest fraction is the solids precipitated between pH 7 and 2. This fraction appears to be comparably small for the #B5 run with KL as feed. Oil fractions after extraction with ethyl acetate are on average 10 wt% with a maximum of 12.8 wt% for the run with LMW fraction as feed. All fractions have their mass balance closed up to ca. 90 wt%, i.e. some systematic mass loss occurs. These compounds are assumed to stay dissolved in the pH 2 aqueous phase without being extracted by the ethyl acetate. A reaction in an autoclave at the same conditions with 30 min retention time did not yield any gaseous products and conducting the recovery process without prior reaction lead to a closed mass balance.

### 3.2.1. GPC, EA, and TGA/DSC

A strong decrease in average  $M_w$  for all fractions for the runs with HMW and KL as feed, while the change for run #B4 with LMW as feed is small (Table 5). The solids precipitated between pH 7 and 2 have a higher  $M_w$  average compared to the solids precipitated at pH 10. Literature mainly shows a decrease in  $M_w$  during base catalysed processes with lignin (Beauchet et al., 2012; Erdocia et al., 2014; Katahira et al., 2016; Lavoie et al., 2011; Mahmood et al., 2013; Miller et al., 2002; Olarte, 2011; Roberts et al., 2011; Schmiedl et al., 2012; Toledano et al., 2014). Definite numbers vary and literature indicates an increase for hardwood organosolv lignin cooked at  $T = 300^\circ\text{C}$  for 40 min (Toledano et al., 2014). Schmiedl et al., 2012 describe the change of  $M_w$  and  $M_n$  graphically indicating a slight decrease over temperature and retention time between 300 and 340 °C and 5 to 15 min.

Elemental analysis demonstrated an increase in carbon content, most pronounced for pH 2 solids (Table 5). The amount of sulphur and oxygen decreased by two thirds and ca. 10% respectively. Beauchet et al., 2012 and Mahmood et al., 2013 observe the same trends for KL treated under hydrothermal conditions. Calculation of the  $C_9$  formulae indicates a decrease by ca. 10 g/mol, the result of a reduction in oxygen content. Using the EA of the feeds and the pH 10 fractions of runs #B3, #B4, and #B5 gives an approximated molecular formula of  $\text{CH}_{2.5}\text{O}_{0.5}\text{S}_{0.1}$  for the 10 wt% missing in the mass balance.

TGA shows that residue at 600 °C increased from 52 wt% for the HMW to 60 wt% for the pH 10 solids and > 65 wt% for the pH 2 solids,

**Table 5**

Molecular weight distribution and elemental analysis data for the feed and #B reactions run – associated comparison between feed types and solids precipitated at different pHs.

Run	Feed			pH 10 solids							pH 2 solids						
	$M_w$ [g/mol]	$M_n$ [g/mol]	PDI [ ]	$M_w$ [g/mol]	$M_n$ [g/mol]	PDI [ ]	C [%]	H [%]	O <sup>a</sup> [%]	S [%]	$M_w$ [g/mol]	$M_n$ [g/mol]	PDI [ ]	C [%]	H [%]	O <sup>a</sup> [%]	S [%]
#B1				2710	600	4.5	63.95	4.93	30.58	0.54	3430	740	4.6	67.24	5.26	27.03	0.47
#B2	7460	1170	6.4	1920	450	4.2	63.11	5.05	31.40	0.44	2770	670	4.1	67.48	5.20	26.82	0.50
#B3				2040	490	4.1	62.94	5.03	31.57	0.46	4320	900	4.8	64.87	5.09	29.65	0.39
#B4	2320	700	3.3	1650	440	3.8	65.56	5.21	28.68	0.55	2150	590	3.6	67.95	5.35	26.14	0.56
#B5	5330	940	5.7	1960	520	3.8	65.08	5.26	29.20	0.46	2370	650	3.7	66.11	5.21	28.21	0.47

indicating that all reactions lead to an increase in thermal stability. The DTG of the KL and the two fractions gave a mono modal distribution with its peak at around 360 °C (Fig. S3). The precipitated solids show a bimodal distribution with one peak at ca. 270 °C and the second at 410 °C.

### 3.2.2. GC MS/GC FID

Table 6 gives the yields of monomeric compounds in the oil phases. Reaction #B1 shows lower amount of the compounds compared to all other. The other reactions with HMW as feed show catechol with a yield of ca. 25 wt% as main product in the oil phase. The compounds being detectable via GC have been estimated with the catechol/syringol response factor to 55–60 wt%. This number is only 35 wt% for the reactions with KL and LMW as feed, hinting at larger molecules in these fractions.

### 3.2.3. ATR FT IR

ATR FT IR of the solids from the reaction of run #B shows some significant differences when compared to the feed (i.e. pH 10 and pH 2 solids of run #B3 compared to their respective feeds; Fig. S6(A)). Band 3 at 1705  $\text{cm}^{-1}$  representing C=O bonds is more pronounced in the pH 10 solids, hinting at an increase in aldehyde groups in this fraction. The pH 2 solids do not have this increase in absorbance, which is one of the few differences in the FTIR spectrum between the pH 10 and pH 2 solids. Absorbance at 1600  $\text{cm}^{-1}$ , (Band #5) representing the symmetric aryl ring stretch, is slightly stronger, while the absorbance of the asymmetric aryl ring stretch (#6) and the asymmetric C–H deformation (#7) at 1510  $\text{cm}^{-1}$  and 1458  $\text{cm}^{-1}$ , respectively, are strongly reduced. In the pH 10 and pH 2 solids no clearly resolved spectral feature at 1426  $\text{cm}^{-1}$  (#8) corresponding to the asymmetric C–H deformation in  $-\text{OCH}_3$  is visible. The latter shifts the minima in absorbance between #8 and #9 to slightly higher wavenumbers. #9 at 1367  $\text{cm}^{-1}$  is again more pronounced, which is the aliphatic CH stretch excluding  $-\text{OCH}_3$ , but including some aromatic skeletal vibrations. #10 is a general aryl ring breathing mode at 1270  $\text{cm}^{-1}$  and is in all samples the strongest absorption. At 1220  $\text{cm}^{-1}$  C=O stretches can be found and this mode absorbs stronger in the pH 10 and pH 2 samples, which is in line with the stronger absorption for #3. #12 and #14 are strongly reduced, both representing guaiacyl ring modes. #13 represents CO in secondary alcohols and aliphatic esters, which could refer to C–OH bonds in side chains of  $\beta$  O 4 moieties or other inter unit connections; these are also



**Table 6**

Monomer yields of the #B runs determined via GC-FID.

Reaction	Oil yield <sup>a</sup> [%]	GC detectables <sup>b</sup> /GC calibrated [%]	Compounds yield <sup>c</sup> [%]				
			Catechol	Guaiacol	Vanillin	4-Methylcatechol	Acetovanillone
#B1	10.51	21.21/16.94	6.29	3.16	2.63	0.82	3.95
#B2	9.29	59.32/50.34	24.71	6.58	5.26	6.09	6.51
#B3	8.54	56.47/46.18	23.59	6.10	4.35	5.43	5.56
#B4	12.80	32.41/26.13	12.37	4.26	2.83	3.05	3.05
#B5	9.91	35.82/28.00	12.15	0.92	4.43	4.35	5.55

<sup>a</sup> Percentage of total.<sup>b</sup> Total mass estimated by total GC-FID area and catechol/syringol response factor.<sup>c</sup> Percentage of total oil.

reduced to a small shoulder. #15 and #16 are vinyl and aromatic CH out of plane vibrations, respectively. The vinyl stretch is removed, while the aromatic one is constant. #17 and #18 are supposed to be CH out of plane vibrations specifically of guaiacyl units. In summary, a strong reduction in absorption between 1270 and 1000 cm<sup>-1</sup> can be observed. These bands mainly correspond to guaiacyl moieties.

### 3.2.4. <sup>13</sup>C cross polarisation magic angle spinning (CP MAS) NMR

<sup>13</sup>C CP MAS NMR spectrum of reaction #B1 pH 10 solids presents resonances at  $\delta_{13C} > 170$  ppm, attributed mainly to the TMSP –COO group (Fig. S6(B)). The aromatic region between  $\delta_{13C} = 160$  and 100 ppm and methoxy groups at  $\delta_{13C} = 56$  ppm show a significant decrease in intensity. The signals in the side chain region for oxygenated aliphatics between  $\delta_{13C} = 100$  and 56 ppm are removed, while those in the region below  $\delta_{13C} = 56$  ppm are decrease, also the other two TMSP associated resonances are to be found. The maxima for the HMW fraction at  $\delta_{13C} = 148.4$  and 124.5 ppm are slightly shifted and less resolved and the methoxy resonance at  $\delta_{13C} = 56$  ppm is reduced to 13%, hinting at demethoxylation and condensation. The comparison between the runs #B1 to #B3 with HMW as feed reveal that run #B3 exhibits a significantly lower signal to noise ratio for as yet unknown reasons (Fig. S7(a)). The peaks are qualitatively comparable to the peaks of runs #B1 and #B2. Fig. S7(d) compares the three different feed types, showing a decrease in total intensity in the order HMW > LMW > KL in the aromatics region. This difference can also be observed for the methoxy groups, while the area between  $\delta_{13C} = 50$  to 0 ppm shows fewer differences in intensity.

## 4. Conclusions

The use of HBCD of KL leads to a decrease in sulphur (by ca. 65%), an increase in carbon content (ca. 10%), with a mass balance of ca. 90 wt%, with ca. 10 wt% remaining in the pH = 2 aqueous phase (after ethyl acetate extraction), with the latter containing 25 wt% catechol. The HMW fraction feed yields higher GC detectable products compared to KL and LMW. NMR analysis highlighted a reduction in aromatics ( $\delta_{13C} = 160$  100 ppm region), side chain removal ( $\delta_{13C} = 100$  60 ppm) and reduction in methoxy resonances ( $\delta_{13C} = 56$  ppm). The thermal stability of all solids was found to increase after HBCD compared to their feeds and a lack of a clear glass transition was observed (similar to that previously reported) (Brodin et al., 2010). Based on this extensive characterisation, the resulting products of the investigated process may be suitable for the synthesis of CF precursors via solvent spinning. To further understand the chemistry of the process, future work will focus on the kinetics of the process and likewise regarding potential industrial engagement, the techno economic feasibility.

## Conflict of interest

This manuscript contains original content that has not been

published previously. There exists no conflict of interest in this manuscript.

## Acknowledgments

RJW acknowledges financial support of the Fraunhofer Society and Fraunhofer Institute for Solar Energy Systems ISE through an “ATTRACT” award. PSS gratefully acknowledges the Spanish Ministry for Economy and Enterprise (MINECO) for a Ramón y Cajal fellowship (RYC 2014 16759) and a proyecto de I+D+I para jóvenes in vestigadores (MAT2014 59674 JIN). RJW and MO would also like to acknowledge the support of the joint Max Planck Society/Fraunhofer Society project “Dendrorefining”. Dr. H. Scherer (AK Krossing; University of Freiburg, Germany) is especially thanked for his assistance with NMR measurements. The authors would like to thank the ICTP CSIC characterisation service for their help in measuring the DSCs of the samples. The Fraunhofer IAP (Potsdam, Germany) is thanked for assistance with GPC measurements.

## References

- Alekhina, M., Erdmann, J., Ebert, A., Stepan, A.M., Sixta, H., 2015a. Physico-chemical Properties of Fractionated Softwood Kraft Lignin and its potential use as a bio-based component in blends with polyethylene. *J. Mater. Sci.* 50, 6395–6406. <https://doi.org/10.1007/s10853-015-9192-9>.
- Alekhina, M., Ershova, O., Ebert, A., Heikkinen, S., Sixta, H., 2015b. Softwood kraft lignin for value-added applications: fractionation and structural characterization. *Ind. Crop. Prod.* 66, 220–228. <https://doi.org/10.1016/j.indcrop.2014.12.021>.
- Baker, D.A., Rials, T.G., 2013. Recent advances in low-cost carbon fiber manufacture from lignin. *J. Appl. Polym. Sci.* 130, 713–728. <https://doi.org/10.1002/app.39273>.
- Baker, D.A., Gallego, N.C., Baker, F.S., 2012. On the characterization and spinning of an organic-purified lignin toward the manufacture of low-cost carbon fiber. *J. Appl. Polym. Sci.* 124, 227–234. <https://doi.org/10.1002/app.33596>.
- Beauchet, R., Montiel-Rivera, F., Lavoie, J.M., 2012. Conversion of lignin to aromatic-based chemicals (L-chems) and biofuels (L-fuels). *Bioresour. Technol.* 121, 328–334. <https://doi.org/10.1016/j.biortech.2012.06.061>.
- Björk, M., Rinne, J., Nikunen, K., Kotilainen, A., Korhonen, V., Wallmo, H., Karlsson, H., 2015. Successful Start-up of Lignin Extraction at Stora Enso Sunila Mill. In: *NWBC 2015. The 6th Nordic Wood Biorefinery Conference: Helsinki, Finland, 20–22 October, 2015*. VTT, Espoo (Finland), pp. 185–192.
- Brodin, I., Sjöholm, E., Gellerstedt, G., 2010. The behavior of kraft lignin during thermal treatment. *J. Anal. Appl. Pyrolysis* 87, 70–77. <https://doi.org/10.1016/j.jaap.2009.10.005>.
- Constant, S., Wienk, H.L.J., Frissen, A.E., Peinder, P.d., Boelens, R., van Es, D.S., Grisel, R.J.H., Weckhuysen, B.M., Huijgen, W.J.J., Gosselink, R.J.A., Bruijninx, P.C.A., 2016. New insights into the structure and composition of technical lignins: a comparative characterisation study. *Green Chem.* 18, 2651–2665. <https://doi.org/10.1039/c5gc03043a>.
- Erdocia, X., Prado, R., Corcuera, M.Á., Labidi, J., 2014. Base catalyzed depolymerization of lignin: Influence of organosolv lignin nature. *Biomass Bioenergy* 66, 379–386. <https://doi.org/10.1016/j.biombioe.2014.03.021>.
- Faix, O., 1992. Fourier transform infrared spectroscopy. In: Lin, S.Y., Dence, C.W. (Eds.), *Methods in Lignin Chemistry*. Springer-Verlag, Berlin, New York, pp. 83–109.
- FAO - Food and Agriculture Organization of the United Nations, 2015. *Pulp and Paper*

- Capacities 2015–2020, Rome.
- Feng, J., Jiang, J., Yang, Z., Su, Q., Wang, K., Xu, J., 2016. Characterization of depolymerized lignin and renewable phenolic compounds from liquefied waste biomass. *RSC Adv.* 6, 95698–95707. <https://doi.org/10.1039/c6ra16916c>.
- Fernandez-Costas, C., Gouveia, S., Sanroman, M.A., Moldes, D., 2014. Structural characterization of Kraft lignins from different spent cooking liquors by 1D and 2D Nuclear Magnetic Resonance spectroscopy. *Biomass Bioenergy* 63, 156–166. <https://doi.org/10.1016/j.biombioe.2014.02.020>.
- Frank, E., Steudle, L.M., Ingildeev, D., Sporl, J.M., Buchmeiser, M.R., 2014. Carbon fibers: precursor systems, processing, structure, and properties. *Angew. Chem. Int. Ed.* 53, 5262–5298. <https://doi.org/10.1002/anie.201306129>.
- Gargulak, J.D., Lebo, S.E., McNally, T.J., 2000. Lignin. In: *Kirk-Othmer Encyclopedia of Chemical Technology*. John Wiley & Sons, Inc., Hoboken, NJ, USA.
- Gellerstedt, G., 2015. Softwood kraft lignin: raw material for the future. *Ind. Crop. Prod.* 77, 845–854. <https://doi.org/10.1016/j.indcrop.2015.09.040>.
- Gellerstedt, G., Tomani, P., Axegård, P., Backlund, B., 2013. Chapter 8. Lignin recovery and lignin-based products. In: Christopher, L. (Ed.), *Integrated Forest Biorefineries. Challenges and Opportunities*. Royal Society of Chemistry, Cambridge, UK, pp. 180–210.
- Gierer, J., 1980. Chemical aspects of kraft pulping. *Wood Sci. Technol.* 14, 241–266. <https://doi.org/10.1007/BF00383453>.
- Hu, Z., Du, X., Liu, J., Chang, H.-M., Jameel, H., 2016. Structural characterization of pine kraft lignin: BioChoice lignin vs Indulin AT. *J. Wood Chem. Technol.* 36, 432–446. <https://doi.org/10.1080/02773813.2016.1214732>.
- Jiang, X., Savithri, D., Du, X., Pawar, S.N., Jameel, H., Chang, H.-M., Zhou, X., 2017. Fractionation and characterization of kraft lignin by sequential precipitation with various organic solvents. *ACS Sustain. Chem. Eng.* 5, 835–842. <https://doi.org/10.1021/acssuschemeng.6b02174>.
- Kadla, J.F., Kubo, S., Venditti, R.A., Gilbert, R.D., Compere, A.L., Griffith, W., 2002. Lignin-based carbon fibers for composite fiber applications. *Carbon* 40, 2913–2920. [https://doi.org/10.1016/S0008-6223\(02\)00248-8](https://doi.org/10.1016/S0008-6223(02)00248-8).
- Katahira, R., Mittal, A., McKinney, K., Chen, X., Tucker, M.P., Johnson, D.K., Beckham, G.T., 2016. Base-Catalyzed depolymerization of biorefinery lignins. *ACS Sustain. Chem. Eng.* 4, 1474–1486. <https://doi.org/10.1021/acssuschemeng.5b01451>.
- Kouisoni, L., Holt-Hindle, P., Maki, K., Paleologou, M., 2012. The LignoForce System™: a new process for the production of high-quality lignin from black liquor. *J. Sci. Technol. For. Prod. Process.* 2, 6–10.
- Kringstad, K.P., Mörck, R., 1983. 13 C-NMR spectra of kraft lignins. *Holzforschung* 37, 237–244. <https://doi.org/10.1515/hfsg.1983.37.5.237>.
- Lake, M.A., Blackburn, J.C., 2014. SLRP™ – an innovative lignin-recovery technology. *Cellul. Chem. Technol.* 48, 799–804.
- Lavoie, J.-M., Baré, W., Bilodeau, M., 2011. Depolymerization of steam-treated lignin for the production of green chemicals. *Bioresour. Technol.* 102, 4917–4920. <https://doi.org/10.1016/j.biortech.2011.01.010>.
- Lupoi, J.S., Singh, S., Parthasarathi, R., Simmons, B.A., Henry, R.J., 2015. Recent innovations in analytical methods for the qualitative and quantitative assessment of lignin. *Renew. Sust. Energ. Rev.* 49, 871–906. <https://doi.org/10.1016/j.rser.2015.04.091>.
- Mahmood, N., Yuan, Z.S., Schmidt, J., Xu, C.B., 2013. Production of polyols via direct hydrolysis of kraft lignin: effect of process parameters. *Bioresour. Technol.* 139, 13–20. <https://doi.org/10.1016/j.biortech.2013.03.199>.
- Mainka, H., Hilfert, L., Busse, S., Edelman, F., Haak, E., Herrmann, A.S., 2015a. Characterization of the major reactions during conversion of lignin to carbon fiber. *J. Mater. Res. Technol.* 4, 377–391. <https://doi.org/10.1016/j.jmrt.2015.04.005>.
- Mainka, H., Täger, O., Körner, E., Hilfert, L., Busse, S., Edelman, F.T., Herrmann, A.S., 2015b. Lignin – an alternative precursor for sustainable and cost-effective automotive carbon fiber. *J. Mater. Res. Technol.* 4, 283–296. <https://doi.org/10.1016/j.jmrt.2015.03.004>.
- Mattsson, C., Andersson, S.-I., Belkheiri, T., Åmand, L.-E., Olausson, L., Vamling, L., Theliander, H., 2016. Using 2D NMR to characterize the structure of the low and high molecular weight fractions of bio-oil obtained from LignoBoost™ kraft lignin depolymerized in subcritical water. *Biomass Bioenergy* 95, 364–377. <https://doi.org/10.1016/j.biombioe.2016.09.004>.
- Miller, J.E., Evans, L.R., Mudd, J.E., Brown, K.A., 2002. Batch Microreactor Studies of Lignin Depolymerization by Bases: 2. Aqueous Solvents. Sandia National Laboratories. Sandia National Laboratories.
- Mörck, R., Yoshida, H., Kringstad, K.P., 1986. Fractionation of kraft lignin by successive extraction with organic solvents: I. Functional groups, <sup>13</sup>C-NMR-spectra and molecular weight distribution. *Holzforschung* 40, 51–60.
- Nagy, M., Kosa, M., Theliander, H., Ragauskas, A.J., 2010. Characterization of CO<sub>2</sub> precipitated Kraft lignin to promote its utilization. *Green Chem.* 12, 31–34. <https://doi.org/10.1039/B913602a>.
- Olarte, M.V., 2011. Base-catalyzed Depolymerization of Lignin and Hydrodeoxygenation of Lignin Model Compounds for Alternative Fuel Production. (PhD, Georgia, USA).
- Otani, S., Fukuoka, Y., Igarashi, B., Sasaki, K., 1969. Method for Producing Carbonized Lignin Fiber.
- Paul, R., Dai, X., Hausner, A., Naskar, A.K., Gallego, N.C., 2015. Treatment of lignin precursors to improve their suitability for carbon fibers: a literature review. In: *Carbon Fibers and Their Composites. Treatment of Lignin Precursors to Improve Their Suitability for Carbon Fibers: A Literature Review*, Oak Ridge, TN, USA. 16–17.04.2015.
- Ragnar, M., Henriksson, G., Lindström, M.E., Wimby, M., Blechschmidt, J., Heinemann, S., 1999–2014. Pulp. In: *Ullmann's Encyclopedia of Industrial Chemistry*. Wiley Interscience, Hoboken, NJ, USA.
- Rencoret, J., Marques, G., Gutiérrez, A., Nieto, L., Santos, J.I., Jiménez-Barbero, J., Martínez, Á.T., del Río, J.C., 2009. HSQC-NMR analysis of lignin in woody (*Eucalyptus globulus* and *Picea abies*) and non-woody (*Agave sisalana*) ball-milled plant materials at the gel state 10th EWLP, Stockholm, Sweden, August 25–28, 2008. *Holzforschung* 63. <https://doi.org/10.1515/HF.2009.070>.
- Rinaldi, R., Jastrzebski, R., Clough, M.T., Ralph, J., Kennema, M., Bruijninx, P.C., Weckhuysen, B.M., 2016. Paving the way for lignin valorisation: recent advances in bioengineering, biorefining and catalysis. *Angew. Chem. Int. Ed.* 55, 8164–8215. <https://doi.org/10.1002/anie.201510351>.
- Roberts, V.M., Stein, V., Reiner, T., Lemonidou, A., Li, X., Lercher, J.A., 2011. Towards quantitative catalytic lignin depolymerization. *Chem. Eur. J.* 17, 5939–5948. <https://doi.org/10.1002/chem.201002438>.
- Samuel, R., Foston, M., Jaing, N., Cao, S., Allison, L., Studer, M., Wyman, C., Ragauskas, A.J., 2011. HSQC (heteronuclear single quantum coherence) <sup>13</sup>C–<sup>1</sup>H correlation spectra of whole biomass in perdeuterated pyridinium chloride–DMSO system: an effective tool for evaluating pretreatment. *Fuel* 90, 2836–2842. <https://doi.org/10.1016/j.fuel.2011.04.021>.
- Schmiedl, D., Endisch, S., Rückert, D., Reinhardt, S., Unkelbach, G., Schweppe, R., 2012. Base catalyzed degradation of lignin for the generation of oxy-aromatic compounds – possibilities and challenges. *Erdoel, Erdgas, Kohle* 128, 357–363.
- Sudo, K., Shimizu, K., 1992. A new carbon fiber from lignin. *J. Appl. Polym. Sci.* 44, 127–134. <https://doi.org/10.1002/app.1992.070440113>.
- Toledano, A., Serrano, L., Labidi, J., 2014. Improving base catalyzed lignin depolymerization by avoiding lignin repolymerization. *Fuel* 116, 617–624. <https://doi.org/10.1016/j.fuel.2013.08.071>.
- Tomani, P., 2010. The lignoboost process. *Cellul. Chem. Technol.* 44, 53–58.
- Tran, H., Vakkilainen, E.K., 2007. The Kraft Chemical Recovery Process. TAPPI - The American Pulp and Paper Industry (Accessed 1 August 2015).

## Repository KITopen

Dies ist ein Postprint/begutachtetes Manuskript.

Empfohlene Zitierung:

Otromke, M.; Shuttleworth, P. S.; Sauer, J.; White, R. J.

[Hydrothermal base catalysed treatment of Kraft Lignin for the preparation of a sustainable carbon fibre precursor.](#)

2018. Bioresource technology reports, 5.

doi:[10.5445/IR/1000090198](https://doi.org/10.5445/IR/1000090198)

Zitierung der Originalveröffentlichung:

Otromke, M.; Shuttleworth, P. S.; Sauer, J.; White, R. J.

[Hydrothermal base catalysed treatment of Kraft Lignin for the preparation of a sustainable carbon fibre precursor.](#)

2018. Bioresource technology reports, 5, 251–260.

doi:[10.1016/j.biteb.2018.11.001](https://doi.org/10.1016/j.biteb.2018.11.001)

Lizenzinformationen: [KITopen-Lizenz](#)